Large-scale forcing of the European Slope Current and associated inflows to the North Sea

Robert Marsh[1], Ivan D. Haigh[1], Stuart A. Cunningham[2], Mark E. Inall[2], Marie Porter[2], Ben I. Moat[3]

[1]Ocean and Earth Science, University of Southampton, National Oceanography Centre, Southampton, European Way, Southampton SO14 3ZH, UK
[2]Scottish Association for Marine Science, Scottish Marine Institute, Oban, Argyll, PA37 1QA, UK
[3]National Oceanography Centre, European Way, Southampton SO14 3ZH, UK

Correspondence to: R. Marsh (rm12@soton.ac.uk)

Abstract. Drifters drogued at 50 m in the European Slope Current at the Hebridean shelf break follow a wide range of pathways, indicating highly variable Atlantic inflow to the North Sea. Slope Current pathways, timescales and transports over 1988-2007 are further quantified in an eddy-resolving ocean model hindcast. Particle trajectories calculated with model currents indicate that Slope Current water is largely "recruited" from the eastern subpolar North Atlantic. Observations of absolute dynamic topography and climatological density support theoretical expectations that Slope Current transport is to first order associated with meridional density gradients in the eastern subpolar gyre, which support a geostrophic inflow towards the slope. In the model hindcast, Slope Current transport variability is dominated by abrupt 25-50% reductions of these density gradients over 1996-1998. Concurrent changes in wind forcing, expressed in terms of density gradients, act in the same sense to reduce Slope Current transport. This indicates that coordinated regional changes of buoyancy and wind forcing acted together to reduce Slope Current transport during the 1990s. Particle trajectories further show that 10-40% of Slope Current water is destined for the northern North Sea within 6 months of passing to the west of Scotland, with a clear decline in this Atlantic inflow over 1988-2007. The influence of variable Slope Current transport on the northern North Sea is also expressed in salinity, which declines through the hindcast period, and there is evidence for a similar freshening trend in observational records. A proxy for Atlantic inflow may be found in sea level records. Variability of Slope Current transport is implicit in mean sea level differences between Lerwick (Shetland) and Torshavn (Faeroes), in both tide gauge records and a longer model hindcast spanning 1958-2013. Potential impacts of this variability on North Sea biogeochemistry and ecosystems, via associated changes in seasonal stratification and nutrient fluxes, are discussed.

1 Introduction

The European Slope Current that lies to the west and north of Scotland exerts considerable influence on the physical and biogeochemical conditions on the adjacent west-European shelf seas (Huthnance et al., 2009). Located above the topographic slope at the eastern boundary, the Slope Current is associated with large-scale density gradients and wind forcing (Huthnance, 1984). Sea surface height drops in the northward direction, while prevailing wind stress is oriented from

southwest to northeast. Density gradients and winds together drive eastward flows towards the slope that are diverted poleward as an intensified geostrophic flow along the slope. The barotropic transport of the Slope Current may be considered buoyancy-forced to first order, modified by frictional influences, with much of the seasonal variability in transport attributed to wind forcing (Huthnance, 1984).

5 The Slope Current is part of the greater flow of Atlantic Water through the Faeroe-Shetland Channel (Sherwin et al., 2008; Richter et al., 2012). Sherwin et al. (2008) identify a long-term mean barotropic transport of 2.1 Sv over the upper part of the slope region of the Shetland shelf. Richter et al. (2012) refer to the flow between the Faeroe and Shetland Islands as the Shetland Current, and use a range of tide gauge data to reconstruct transports in the region. Interestingly, they are unable to reconstruct Shetland Current transports, an issue that we return to in the discussion.

10 The North Sea has warmed considerably since the late 1980s, to an extent considered unprecedented in the historical record (MacKenzie and Schiedek, 2007). In addition to warming, there is some evidence for surface freshening over the 1990s (e.g., Fig. 3a in Hjøllo et al., 2009). Recent warming of the North Sea follows a wider pattern of warming across Europe, and increasingly mild winters in particular (MacKenzie and Schiedek 2007), although major inflows of warm Atlantic Water in 1988 and 1998 are also believed to have contributed to the warming (Reid et al., 2001).

15 Episodic changes in Atlantic inflow have been attributed to anomalous wind forcing, hence wind-driven changes in Atlantic inflow and the associated warming have been a focus of recent model studies. Hjøllo et al. (2009) use a numerical model of the North Sea region to investigate changes of heat content over 1985-2007, in particular a long-term warming of 0.62°C. Dividing the North Sea into northern and southern circulation regimes, they find that inflows at the northern boundary are strongly influenced by large-scale atmospheric forcing associated with the North Atlantic Oscillation, but that variable

20 inflow at open boundaries has a limited direct influence on heat content variability. Winther and Johannessen (2006) relate changes of Atlantic inflow to wind forcing, but also emphasize the dilution of Atlantic Water as it circulates the North Sea before leaving in the Norwegian Coastal Current.

Interannual variability in the European Slope Current has recently been explored using altimetry data over a 20-year period, revealing a peak in poleward flow along much of the continental slope from Portugal to Scotland during 1995–1997, and a

25 long term decreasing trend of ~ 1% per year (Xu et al., 2015). Here, we consider the extent to which changes in the Atlantic inflow to the North Sea are associated with variability of the Slope Current driven by changing large-scale meridional density gradients and winds. We use a wide range of observations and eddy-resolving model hindcast data to examine the Slope Current, large-scale forcing mechanisms, and Atlantic inflow to the North Sea.

The paper is organized as follows. In Sect. 2, we outline the variety of data and methods used. In Sect. 3, we evaluate

30 simulated Slope Current drift over 1995-1997 using archived drifter data (Sect. 3.1). We then characterize Slope Current pathways, timescales and transports in a model hindcast spanning 1988-2007 (Sect. 3.2). With considerable Slope Current variability evident in the hindcast, we consider the influence of two large-scale driving mechanisms, meridional density gradients and wind forcing (Sect. 3.3), in both the model and observations. Finally, we explore the evidence for variable Slope Current influences on the North Sea (Sect. 3.4), and a proxy for Atlantic inflow to the North Sea based on the sea level

gradient between Shetland and the Faeroes (Sect. 3.5). In discussion and conclusion (Sect. 4), we suggest that variations in Slope Current transports and the Atlantic Water influence on the North Sea are primarily linked to variable meridional density gradients in the eastern subpolar gyre that are attributed to the combined (reinforcing) effects of wind and buoyancy forcing.

5 2. Datasets and Methodology

In Sect. 2.1, we introduce the drifter data used to provide an observational perspective on the Slope Current system, and for preliminary evaluation of model drift. In Sect 2.2, we outline the model hindcasts used to characterize variability of the Slope Current system. In Sect. 2.3, we outline the Lagrangian diagnosis of hindcast data: the ARIANE methodology for calculation of particle trajectories based on velocity fields, and the accompanying statistical analyses. We then introduce the
10 observations used to explore forcing mechanisms: mean absolute dynamic topography and climatological density data (Sect. 2.4); wind stress reanalysis data (Sect. 2.5). Finally, in Sect. 2.6 we introduce the tide gauge data and analysis used to explore Slope Current transport between Shetland and the Faeroes.

2.1 Drifter data

As part of the Land-Ocean Interaction Study (LOIS), the Shelf Edge Study (SES) was undertaken in the mid-1990s. LOIS-
15 SES included two Slope Current drifter experiments within which drifters were released in three groups of seven in an east-west line 20 km long across the continental shelf west of Scotland near 56.25°N, on 5 December 1995 and on 5-9 May 1996 (Burrows and Thorpe, 1999; Burrows et al., 1999), to characterize winter and summer conditions. The drifters were drogued at a depth of 50 m and tracked for up to 240 days, to study the regional circulation and dispersion. The archived drifter positions from both experiments are using to provide some context for the study, and for a basic evaluation of corresponding
20 drift in the model (see below).

2.2 Model hindcasts

We sample currents and hydrographic data (temperature, salinity) from the northeast Atlantic region of an eddy-resolving (1/12°) global ocean model hindcast (the ORCA12 configuration of NEMO) for the period 1988-2007 (see Blaker et al., 2015), henceforth ORCA12-N01. NEMO (Madec, 2008) is a state-of-the-art, portable ocean modelling framework
25 developed by a consortium of European institutions. We use results for the hindcast period to simulate region-typical patterns of particle drift and dispersal (see methods). Our choice of this hindcast is guided by evidence that eddy-resolving simulations can faithfully reproduce the global EKE field observed with satellite altimetry (Petersen et al., 2013), while lower-resolution eddy-permitting simulations are known to substantially underestimate EKE (McClean et al., 2002; Hecht and Smith, 2013). NEMO is forced with 6-hourly winds supplied by the DFS4.1 (1988-2006) and DFS5.1.1 (2007-2010)
30 datasets (Brodeau et al., 2010). The hindcast provides 5-day averages of the eddying "surface currents", a time window

appropriate to model realistically and with high precision the advection of an ensemble of particles representative of Slope Current transport. Most recently, a longer hindcast simulation with ORCA12 became available (e.g., Moat et al., 2016), henceforth ORCA12-N06, and we use diagnostics from this experiment to extend our analysis to the longer period 1958-2012.

2.3 Lagrangian model diagnostics

We use the ARIANE particle-tracking software (Blanke and Raynaud 1997) to track ensembles of particles that are "seeded" in the northward-flowing Slope Current. We release 630 particles, at 30 model levels from 9.85 m down to 371.22 m, and at 21 equally-spaced locations across a short section on the ORCA12 mesh (9.46°W 55.83°N to 9.28°W 55.82°N). Release points are close to where floats have been deployed as part of the UK NERC project FASTNEt (http://www.sams.ac.uk/fastnet). Particles are released on 1 January or 1 July, to sample the two halves of the seasonal cycle, with location, depth and ambient water properties (temperature, salinity) recorded every 24 hours for 183 days. Particle locations are statistically analysed to obtain a measure of particle density, dividing the number of particle occurrences in a limited longitude-latitude range by the total number of particle occurrences during the tracking period. We use a 0.5° x 0.5° mesh to sample for particle occurrence, optimal for both the resolution of the Slope Current and sampling of sufficient particles from a statistical perspective. This quantifies interannual variation in pathways, broadly distinguishing between years of low and high influence of the Slope Current on the northern North Sea. Alongside this particle density, we also obtain an average particle age (since release) per 0.5° x 0.5° grid cell, to quantify variations in travel time.

2.4 Mean absolute dynamic topography (MADT) and climatological density

Daily global absolute sea-surface dynamic topography distributions with a spatial resolution of 0.25° are produced by Centre National d'Etudes Spatiales (CNES), and distributed through AVISO+ (http://www.aviso.altimetry.fr). Here, we use Delayed Time data from the SSALTO/DUACS system (AVISO+, 2014), which provides a homogeneous, inter-calibrated time series of sea-level anomaly. Absolute sea surface dynamic topography is the sum of sea level anomalies and a mean dynamic topography, both referenced over a twenty-year period (1993-2012). Key improvements in this new dataset are the use of a new mean dynamic topography (MDT CNES_CLS13) calculated from GOCE satellite data, increased use of in-situ observations over the longer reference period, and more accurate mapping of the mesoscale (Rio et al., 2011). The geoid model developed from the GOCE satellite data has a horizontal resolution of 125 km. Multivariate objective analysis (including wind and in situ data) is used to improve the large-scale solution, resulting in a final gridded horizontal resolution of 0.25°.

Monthly estimates of ocean temperature and salinity spanning the same period are available as objectively-analysed gridded fields from the EN4 dataset provided by the UK Met Office Hadley Centre (Good et al., 2013). EN4 comprises global gridded fields of potential temperature and salinity at 1° resolution with 42 vertical levels. From 2002, the Argo float programme significantly improved EN4 data coverage in the northeast Atlantic (Good et al. 2013). The gridded temperature

and salinity estimates are used to calculate climatological potential density referenced to the surface (σ_0), at selected depth levels. Of specific relevance to the Slope Current, and the present study, are meridional gradients of MADT and potential density.

2.5 Wind stress data

5 For the study period 1988-2007, we obtain 10-m winds from the ERA-interim 12-hourly, 0.75° x 0.75° resolution reanalysis datasets (Dee et al., 2011). We calculate wind stress following the methods of Large and Pond (1981). To address wind forcing of the Slope Current, a slope-based subset is extracted from the wind stress field between the 200 m and 1000 m contours (bathymetry from ETOPO1, Amante and Eakins, 2009) in the latitude range 48-60°N. These wind stress vectors are rotated into a coordinate system parallel to the 500 m contour and then averaged to obtain annual-mean averages over 1988-

10 2007.

2.6 Tide gauge data

Monthly mean sea level records were obtained from the Permanent Service for Mean Sea Level (PSMSL; http://www.psmsl.org) for tide gauges at Lerwick (Shetland; 1.14°W, 60.15°N) and Torshavn (Faeroes; 6.77°W, 62.01°N) (Holgate et al., 2013; PSMSL, 2015). The Lerwick record spans the period 1957-2014 and is 91% complete. The Torshavn

15 record spans the period 1957-2006, and is 84% complete. Records were corrected for the effects of glacial isostatic adjustment (GIA), using the ICE-5G model results available from the PSMSL. We calculate the difference in sea surface height between the two tide gauge records (after correcting for GIA) and use this as a proxy for Slope Current transport. Note that the tide gauge records are referenced to different local datums and within the scope of this study it has not been possible to directly tie these together. However, because we are interested in the interannual variability of the Slope Current,

20 we just consider the relative difference in sea surface height between the two sites.

3. Results

3.1 Drifter observations and ORCA12 simulations of Slope Current pathways, 1995-97

To provide some context for the study, and a basic evaluation of corresponding model drift, in Fig. 1 we show LOIS-SES drifter data alongside example model particle trajectories. LOIS-SES drifter deployments in December 1995 (Fig. 1a) and

25 May 1996 (Fig. 1b) reveal somewhat different pathways in and around the Slope Current, with a tendency for more extensive drift in winter releases, compared to summer releases. Most drifters follow the Slope Current for several hundred kilometres following release in December 1995. Several drifters enter the northeast sector of the North Sea by late winter or early spring, a travel timescale of 2-3 months. In contrast, several drifters released in May 1996 move onto the shelf and directly to the northwest North Sea, but on a wide range of timescales due to highly variable shelf currents.

Model particle trajectories start on 1 January and 1 July 1996 (Fig. 1c,d) at the FASTNEt section, and are tracked forwards for 6 months. Particles released on 1 January tend to disperse more widely than those released on 1 July, with a larger number reaching the northwest and northeast sectors of the North Sea within 6 months. There are limitations to the direct comparison of the drifters and particle trajectories, as the former are more limited in number and subject to sub-mesoscale processes and tides that are not represented in the model. However, in broad terms, model particle trajectories indicate drift pathways and timescales similar to the drifters, and suggest more extensive drift in the first half of 1996, compared to the second half, that is consistent with the observations and indicative of known seasonality in Slope Current dynamics.

3.2 Characterizing Slope Current pathways, timescales and transports in the ORCA12 hindcast of 1988-2007

As outlined in Sect. 2, particle density and mean age maps are obtained on a 0.5° x 0.5° mesh for each year from 1988-2007 (see Figs. S1-S4 for 1 July starts). The statistics for each set of 20 ensembles (January/July releases, tracked forwards/backwards) are further averaged to obtain the "grand ensemble" results shown in Figs. 3 and 4, respectively.

Tracking forwards, Fig. 2 shows the "grand mean" of particle density and age, for particles released on 1 January (Fig. 2a,c) and 1 July (Fig. 2b,d). Ages are expressed as days since 1 January or 1 July. Particle density is simply the fraction of all particle positions in each 0.5° x 0.5° grid square, in relation to all particle positions. With variation across three orders of magnitude, we use a log scale to highlight the distribution of this statistic. Highest particle density (~0.1) and youngest age (0-20 days) is naturally located near the release section. Relatively high particle density otherwise traces the Slope Current pathway, characteristically following the shelf break (see Fig. 1), but bifurcating to the northeast of Scotland and just west of Norway. Only a small fraction of particles are tracked further to the northwest and a destination in the Norwegian Sea. Back upstream, particles can also follow a minor pathway offshore to the north of the release section, turning westward to the south of Iceland and then southward along the Reykjanes Ridge. Another minor pathway involves almost immediate recirculation to the west of Ireland. Within 6 months, a few particles reach domain boundaries, to the north, east and west. With the focus of this study on the northern North Sea, these boundary terminations are not problematic.

Turning to the mean age of particles, this correspondingly increases to 140-180 days at locations most remote from the release section. There are relatively small differences between the January and July releases, although it appears that particles released in January reach the northwest North Sea more quickly, and in larger numbers. Mean ages for January releases are younger by ~10 days at many locations, suggestive of a more vigorous circulation during the first half of the year and more extensive shelf edge exchange, with higher on-shelf particle densities in particular.

Tracking backwards, Fig. 3 shows the corresponding particles density and age distributions for flows feeding transport across the FASTNEt section. Similar to the results for forward tracking, highest particle densities are located adjacent to this section. In contrast to the forward tracking, particle density is generally lower across a broader area of the eastern subpolar gyre, indicative of a widespread inflow across the approximate latitude range 48-60°N. As for forward tracking, a few back trajectories reach the western domain boundaries in a little under 180 days. There is some evidence for a southward continuation of the Slope Current, along the shelf break, to around 13°W, 48°N. This is more evident in back-trajectories that

span the second half of the year (i.e., reaching the FASTNEt section in January). This "upstream" branch of the Slope Current is slower than the "downstream" branch represented in Fig. 2, consistent with downstream strengthening of Slope Current transport through progressive inflow from the west.

We now consider the corresponding changes in Slope Current transport at selected locations along the shelf break. Figure 4

5   shows Slope Current transport every 5 days over 1988-2007 at the FASTNEt, EEL and Shetland Slope sections (see Fig. 1c,d). Designation of the two downstream sections (EEL and Shetland Slope) is based on the location of the Slope Current in ORCA12, rather than strict delimitation by the same isobaths (model bathymetry) spanned at the FASTNEt section (333 m to 1387 m). Hence the EEL section spans a depth range 199-1796 m, while the Shetland Slope section spans 133-412 m. On this basis, we diagnose Slope Currents transports in observed ranges (e.g., Sherwin et al., 2007). Between the FASTNEt and

10 Shetland Slope sections, long-term mean transport increases, while the standard deviation decreases, from 2.79 ± 1.68 Sv to 4.72 ± 1.44 Sv (Table 1).

As a metric of seasonal variations in transport, we sample the ensemble-mean particle ages in Fig. 2 for travel times between sections. These are shorter and less variable in the first half of the year: 19.4 ± 7.7 days (January releases) compared to 28.7 ± 20.4 days (July releases) between FASTNEt and EEL sections; 90.4 ± 23.7 days (January releases) compared to 98.6 ±

15 32.3 days (July releases) between FASTNEt and Shetland Slope sections (Table 1). This is consistent with a somewhat more vigorous circulation during January-June, most clearly evident in the time series of Shetland Slope transports (Fig. 4c).

Regarding the 1988-2007 variability in Fig. 4, a general impression is that transports are weaker in the second decade of the hindcast, with a most striking shift to weaker transport at the EEL section over 1996-1998. To investigate the extent to which Slope Current transport variability (including the seasonal cycle) is instantaneously correlated at the three sections, we

20 compute correlations between the 5-day averaged transports in Fig. 4, confirming that variability along the shelf break is coordinated to an extent. This is most evident between the FASTNEt and EEL sections, for which the correlation is 0.64 (significant at 99% confidence level), as might be expected given the relatively short distance separating these two sections. More striking is a correlation of 0.43 (significant at 99% confidence level) between transports at the more widely separated EEL and Shetland Slope sections.

25 **3.3 Mechanisms driving Slope Current variability**

We consider in turn the influences of meridional density gradients to the west of the shelf break, and the local winds along the shelf break, in driving the variability in Slope Current transport evident in the ORCA12 hindcast.

3.3.1 Meridional density gradients

To first order, the Slope Current is driven by the deep ocean meridional density gradient. We can accommodate this in the

30 geostrophic momentum balance, as presented in Simpson and Sharples (2012) and reproduced here. First consider the zonal momentum equation, given reference density ρ_0 and Coriolis parameter f. We use the hydrostatic balance, whereby pressure

$p = \rho g(z + \eta)$, given density ρ, gravitational acceleration g, arbitrary ocean depth z and sea surface elevation η, and we assume that the zonal density gradient is zero. The right hand side thus simplifies to a zonal gradient in sea surface height:

$$-fv = -\frac{1}{\rho_0}\frac{\partial p}{\partial x} = -\frac{1}{\rho_0}\frac{\partial(\rho g(z+\eta))}{\partial x} = -g\frac{\partial \eta}{\partial x}, \tag{1}$$

Vertically integrating in the depth range $-h$ and η, defining meridional transport, $V = \int_{-h}^{\eta} v \, dz$, and assuming $h \gg \eta$, the depth-integrated zonal momentum balance follows as:

$$-fV = -g\frac{\partial \eta}{\partial x}h, \tag{2}$$

Considering the y-momentum equation, we follow the same approach, noting that the meridional density gradient is non-zero, so the right hand side now includes an extra term:

$$fu = -\frac{1}{\rho_0}\frac{\partial p}{\partial y} = -\frac{1}{\rho_0}\frac{\partial(\rho g(z+\eta))}{\partial y} = -\frac{g}{\rho_0}\frac{\partial \rho}{\partial y}z - g\frac{\partial \eta}{\partial y}, \tag{3}$$

Vertically integrating again, defining zonal transport, $U = \int_{-h}^{\eta} u \, dz$, the meridional momentum balance follows as:

$$fU = -\frac{g}{2\rho_0}\frac{\partial \rho}{\partial y}h^2 - g\frac{\partial \eta}{\partial y}h, \tag{4}$$

Cross-differentiating (2) and (4) for $\partial U/\partial x$ and $\partial V/\partial y$, and given vertically-integrated continuity of volume, $\partial U/\partial x + \partial V/\partial y = 0$, we obtain an expression for the meridional gradient in sea surface elevation as a function of local depth (h) and the meridional density gradient:

$$\frac{\partial \eta}{\partial y} = -\frac{h}{\rho}\frac{\partial \rho}{\partial y}, \tag{5}$$

We further distinguish between the shelf (depth $h = h_s$) and the deep ocean ($h = H$):

Shelf: $$\left(\frac{\partial \eta}{\partial y}\right)_{h_s} = -\frac{h_s}{\rho}\frac{\partial \rho}{\partial y}, \tag{6}$$

Deep ocean: $$\left(\frac{\partial \eta}{\partial y}\right)_H = -\frac{H}{\rho}\frac{\partial \rho}{\partial y}, \tag{7}$$

Applying this theoretical framework, we use MADT and climatological temperature and salinity observations to evaluate the meridional gradients of Eq. (7) in the eastern subpolar North Atlantic, where the Slope Current originates (Fig. 3). Fields of MADT and mean σ_0 at 500m (Fig. S5a,b) are broadly characterized by negative and positive meridional gradients respectively (Fig. S5c,d). Dividing $\partial \eta/\partial y$ by $-\rho^{-1}\partial \rho/\partial y$, we obtain an estimate of the deep ocean depth scale H, plotted in Fig. 5. Over large areas of the region, H is thus predicted in the range 500-2500 m, representative of the deep ocean.

Since $H >> h_s$, Eqs. (6) and (7) predict that the (downward) meridional gradient in η will be greater over the deep ocean than over the shelf, so the cross-slope (downward) gradient in η increases with latitude (see also equation pair 10.11 in

Simpson and Sharples, 2012). This cross-slope difference in sea surface elevation will result in a geostrophic current parallel to the isobaths. At the same time, the momentum balance in the meridional direction implies a geostrophic transport in deep water towards the slope, predicted by substituting Eq. (7) into Eq. (4):

$$U = \frac{gH^2}{2\rho_0 f}\frac{\partial \rho}{\partial y},$$

(8)

5 As this zonal flow reaches the slope, it turns to the north and joins the meridional current. This current increases with latitude as the zonal difference in height across the sloping seabed, which increases likewise (see also equation 10.12 in Simpson and Sharples, 2012). Using Eq. (8) with g = 9.81 m^2 s^{-1}, ρ_0 = 1025 kg m^{-3}, representative latitude 55°N (f ~ 1.19 x 10^{-4} s^{-1}), and H = 1000 m as a depth scale appropriate for the inflow (from Fig. 5), we obtain U ~ 8 x 10^7 $\partial \rho/\partial y$, (m^3 s^{-1} per m along slope). Considering the Slope Current to be thus "fed from the west" by geostrophic inflows that are supported by a meridional

10 density gradient, we now investigate how this large-scale pattern may have changed over the hindcast period. Supplementary Figs. S6 and S7 show maps of potential density (σ_0) for 1-5 January, biennially over 1988-2006, at two depth levels - 500 m and 947 m - which are representative of the inflow. At 500 m, it is evident that density to the south of Iceland progressively decreases over 1988-2006; at 947 m there is a progressive increase of density at mid-latitudes over the study period, with little change further to the north. Both changes result in a reduction of the northward density gradient.

15 Variability of $\partial \rho/\partial y$ is more explicitly shown in Fig. 6 as northward trends of σ_0 over the latitude range 45-62°N, in the northeast Atlantic (across 15-28°W), 5-daily for 1988-2007, at 500 m (Fig. 6a) and at 947 m (Fig. 6b). Reductions in the trend are evident throughout most of the period, with particularly abrupt reductions over 1995-1997 and overall reductions in the range 25-50%, with strongest % reductions in the east (around 15°W). These abrupt changes are consistent with the sharp reduction of Slope Current transport at the FASTNEt and EEL sections (Fig. 4a,b).

20 As a metric for density forcing of the Slope Current, we average the 45-62°N density gradients across 15-28°W and annually, and then take annual anomalies relative to the 20-year mean. Figure 7 shows 1988-2007 time series of these metrics for density gradients at 500 m (Fig. 7a) and at 947 m (Fig. 7b). The annual index clearly shows how the density gradients weakened around the mid-1990s. Taking a change in $\partial \rho/\partial y$ of 2-4 x 10^{-3} kg m^{-3} degree^{-1} (111 km), Eq. (8) suggests a change of inflow, ΔU ~ 8 x 10^7 x [2-4] x 10^{-3} x (111 x 10^3)$^{-1}$ = 1.42-2.9 m^2 s^{-1}. Across 17° of latitude, this amounts

25 to a change (decrease) of total inflow in the range 2.75-5.5 Sv, broadly consistent with the abrupt drop in transport, over 1996-1998, at the EEL section in particular (Fig. 4b).

In Fig. 7c and 7d, we plot these metrics against annual-mean SC transports at the EEL section. We find strong and significant correlations, of up to 0.74 and 0.84 (both significant at 99% confidence level) between Slope Current transport at the EEL section and the density gradient indices, at 509 m and 947 m respectively. Somewhat weaker correlations, although

30 still significant at 99% confidence level, are obtained between the density gradient indices and annual-mean transports at the Shetland Slope section (0.64 at 509 m; 0.59 at 947 m) and at the FASTNEt section (0.68 at 509 m; 0.73 at 947 m). Strongest

correlations at the EEL section are associated with a degree of bimodal scatter in Figs. 7c,d, associated in turn with abrupt declines of density gradients (Fig. 7a,b) and Slope Current transport (Fig. 4b) in the mid 1990s.

3.3.2 Wind forcing

While density gradients do indeed appear to exert a leading control on barotropic Slope Current transport, wind forcing is

5   also likely to play an important role on short timescales. In particular, strong wintertime winds likely explain strongest Slope Current transport at that time of the year (Huthnance, 1984). For a circular basin with a sloping margin and wind-stress forcing, Huthnance (1984) uses scaling arguments applied to incompressible, hydrostatic momentum equations (with horizontal flow scales > topographic slope scale and vertical scales; and w << u) to demonstrate that in a steady state, any component of wind stress parallel to a steep slope (τ^s) will induce a downwind current along the continental shelf and slope,

10   with a speed given by $\tau^s/(\bar{\rho}k)$, where $\bar{\rho}$ is a depth mean density and k is a linearized friction coefficient. Additionally, applying a uniform azimuthal density gradient, and similar scaling arguments, a slope/shelf current (in the direction of decreasing sea surface height) will have strength comparable to the wind-stress induced current if:

$$\frac{\partial \rho}{\partial s} = \frac{A}{hHg}|\tau^s|,\qquad(9)$$

where $\partial \rho / \partial s$ expresses the depth-mean along-slope density gradient, A = 2 to 4 (dependent on scaling assumptions) and h

15   and H are the local and maximum water depths (see Huthnance 1984, un-numbered equation, end of p.799).

In interpreting these scaling arguments as applied to the eastern margin of the North Atlantic, the underlying physics is such that in a steady sense both the eastward geostrophic flow (derived from the meridional density gradient), and an eastward surface Ekman response (derived from a northward wind-stress) drive water initially towards the closed eastern boundary. These eastward flows raise the sea level near the eastern boundary, and result in a geostrophically balanced northward flow,

20   with friction balancing the down-wind and down-pressure gradient accelerations.

Although unimportant when making a relative comparison between wind stress and buoyancy forcing, the linearized friction coefficient determines the absolute strength of the northward current (for given forcing). Expressed as $k \propto U_{M2}/h$ (where U_{M2} is a magnitude for the semi-diurnal tidal current speed), friction therefore determines the zonal structure of a Slope Current (moving across the slope). In the setting of the shallow and strongly tidal northwest European shelf, friction is

25   greatest on the shelf, and the strongest northward flows are therefore concentrated over the slope.

The effects of seasonality in a northeast Atlantic setting are noteworthy. In winter, the surface Ekman layer will be deeper than the shelf break, and the eastward Ekman mass convergence will manifest at least in part over the continental slope. Both eastward Ekman and eastward geostrophic flow (in balance with the meridional density gradient) therefore have co-located convergence over the slope in winter, forcing a strong and mostly barotropic Slope Current. In summer, by contrast, the

30   surface Ekman layer will be considerably shallower than the shelf break, with convergence occurring more towards the

coast. This leads to greater surface water exchange onto the shelf, and a more spatially diffuse northward flow over the slope and shelf, since the effects of wind-stress and meridional buoyancy forcing are no longer co-located over the slope.

Here, we focus on interannual changes in wind forcing, considering the influence on Slope Current transport of anomalies in along-slope wind stress. As a metric for the wind-stress forcing of the Slope Current, and for direct comparison with the density gradient metric developed in Sect. 3.3.1, we evaluate the right hand side of Eq. (9) annually over the continental slope between 48-62°N, where $|\tau_s|$ is obtained from re-analysis 10 m winds, as outlined in Sect. 2.5. Expressed in units of northward density gradient (10^{-3} kg m^{-3} degree^{-1}, regressed in the latitude range 48-62°N), annual anomalies of this metric are shown in Fig. 8. The anomalies are generally smaller in magnitude compared to the large-scale anomalies in Fig. 7, but there is a similar tendency for positive (negative) anomalies before (after) 1996 (as Fig. 7). In Sect. 4, we discuss the combined influences of wind and buoyancy forcing on variable Slope Current transport, as diagnosed with this common framework.

3.4 Variable Slope Current influences on the North Sea

Returning to the Lagrangian analysis, and noting the tendency for particles to separately branch into the northwest and northeast North Sea (see Fig. 2), we consider the percentage of particle counts in sub-regions bounded 4.5°W to 1.5°E, south of 59°N (the "NW North Sea"), and east of 1.5°E, south of 62°N (the "NE North Sea"). For each year over 1988-2007, we average these statistics for both January and July releases. Figure 9 shows histograms of this annual mean %, for each sub-region and both combined. In terms of a combined presence in the North Sea, the % of particles released at the FASTNEt section declines from near 40% in the early 1990s to around 15% in the mid 2000s. This long-term decline is suggestive of a reduced influence of Slope Current water of Atlantic origin in the northern North Sea, in the ORCA12 hindcast. The decline is similarly evident in the separate January and July releases (not shown), indicating a year-round character.

As an independent measure of the presence of water derived from the Slope Current in the northern North Sea, we further consider salinity. For the NW and NE North Sea in the model hindcast, Fig. S8 shows the area-averaged surface salinity (top left panels), corresponding mean seasonal cycles (top right panels), and anomalies (bottom panels). The seasonal cycle of surface salinity in the northeast North Sea is strongly influenced by the expansion and contraction of the Norwegian Coastal Current that is an extension of very fresh outflow from the Baltic Sea. Figure 10 shows annually averaged surface salinity anomalies, indicating a general decline in salinity, in both sub-regions, consistent with a reduced presence of Atlantic Water. We note evidence for similar surface freshening over the 1990s in observations in the central North Sea at station Terschelling, and at the Norwegian coastal station Ytre Utsira (e.g., Fig. 3a in Hjøllo et al., 2009). Temperature in contrast (not shown) is more variable at interannual timescale, influenced to a large extent by local surface net heat fluxes (Sharples et al., 2006).

The long-term freshening trend coincides to an extent with declines in Slope Current transport and the fraction of particles reaching the North Sea. A correlation coefficient of 0.53 between annual-mean salinity anomalies in the NE North Sea and Slope Current transport at the Shetland Slope is significant at the 95% confidence level. However, NW North Sea salinity

anomalies and Shetland Slope transports are not significantly correlated at the same confidence level (r = 0.30). This may be due to our fixed definition of Slope Current transport along the Shetland Shelf break; during years of stronger transport, additional on-shelf transport may supply higher salinity water to the NW North Sea, explaining a substantial fraction of the variability in Fig. 10a.

5   ### 3.5 A proxy for Slope Current transport and Atlantic inflow to the North Sea

As Slope Current transport is strongly barotropic, we expect a strong correlation with the sea surface difference across the current. Given the available tide gauge data at Lerwick and Torshavn (Sect. 2.6), we consider the difference in relative sea surface height (SSH) between Shetland and the Faeroes in ORCA12. For the 1988-2007 hindcast, Fig. 11a shows 5-day averages of SSH at the nearest ocean grid cell to Lerwick (red curve) and Torshavn (blue curve), and the difference (Lerwick
10   minus Torshavn, Fig. 11b). There is a clear seasonal cycle in SSH at both locations, with higher (lower) SSH in summer (winter), largely due to the thermosteric effect of winter cooling (summer warming) and contraction (expansion) of water columns. The seasonal cycle reaches higher amplitude at Lerwick, hence there is also a seasonal cycle in the SSH difference, with larger differences in winter. There is also an impression of generally smaller SSH differences later in the 20-year hindcast.

15   Removing mean seasonal cycles in Shetland Slope transport and SSH difference from 5-day averaged data, we find that transports are strongly correlated with SSH differences (r = 0.79, significant at 99% confidence level; linear regression ~0.2 Sv per cm), indicating how SSH differences may be useful as a direct proxy for Slope Current transports. Annual-mean anomalies are shown in Fig.12. More negative anomalies, of both transport (Fig. 12a) and SSH difference (Fig. 12b), are apparent during the second decade of the hindcast.

20   To relate changes in SSH difference, Slope Current transport, and the Atlantic inflow to the North Sea, we correlate the "combined" % of North Sea particles (Fig. 9c) and the annual-mean anomalies in Fig. 12. Correlation coefficients of 0.57 (with transports) and 0.70 (with SSH differences), both significant at 99% confidence level, indicate that larger SSH differences and stronger transport are indeed associated with more water of Slope Current origin reaching the North Sea. The stronger correlation of % North Sea particles with SSH difference (compared to transport) indicates that this metric more
25   completely captures transport variability than the fixed Shetland Shelf section. Clearly then, declining Slope Current transport across the Shetland Shelf over 1988-2007 is broadly representative of changes already evident in the wider (upstream) Slope Current system, and consistent with the declining % of Slope Current water particles reaching the North Sea.

Evidence for variable Slope Current transport over a longer time period is now considered, using historical tide gauge data
30   and the longer ORCA12-N06 hindcast. Figure 13 shows SSH at Lerwick and Torshavn from 1957 onwards in tide gauge records, after correcting for GIA (Fig. 13a), from 1958-2013 in the ORCA12-N06 hindcast (Fig. 13b), and the corresponding SSH differences (Fig. 13c). Considering the SSH records (Fig. 13a,b), there is general agreement between the tide gauges and ORCA12 in terms of a seasonal cycle and long-term sea level rise primarily associated with thermal expansion, although

irreconcilable differences currently remain between the datum levels for the two tide gauge records (therefore Fig. 13a and Fig. 13b should not be directly compared).

Considering SSH differences (Fig. 13c), ORCA12-N06 indicates a degree of low-frequency variability, with smaller SSH differences in the last ~15 years (in close agreement with ORCA12-N01 over the period of overlap - see Supplementary

5   Material, Fig. S9), seen to an extent in the tide gauge record whenever the data is available. The ORCA12-N06 hindcast is regarded as more reliable after a short spin-up period, so we consider correlations between model and observations both including and excluding the simulation prior to 1970. Correlation coefficients between tide gauge difference and model SSH difference are 0.50 (all data) and 0.66 (post-1970 data), both significant at 99% confidence level. These preliminary findings help to validate the Slope Current variability simulated in ORCA12 hindcasts, and establish the potential for further

10   investigation of variable Slope Current transport and Atlantic inflow to the North Sea over the longer historical era.

4. Discussion and Conclusions

The Slope Current system that is observed to follow the shelf break to the west and north of Scotland is investigated using a range of observations and an eddy-resolving ocean model (ORCA12) hindcast spanning 1988-2007. Deployments of drogued drifters over 1995-1997 reveal a variety of pathways and timescales in the Slope Current system, hinting at seasonal

15   to interannual variations. To further explore this variability, offline particle trajectories are calculated with model currents. Particles are tracked both forwards and backwards in time, for 183 days, from a section across the Slope Current (9.46-9.28°W at ~55.82°N, in the upper 371 m) where floats have been deployed as part of the UK NERC project FASTNEt (http://www.sams.ac.uk/fastnet). Tracked backwards, particle trajectories reveal a major source of Slope Current water in the eastern subpolar gyre, with a smaller proportion advecting with the Slope Current from more southern latitudes.

20   Variable pathways are related to both seasonal and interannual variability in Slope Current transport. The latter variability is related to large-scale forcing mechanisms. Downward trends in Slope Current transport, similar to those inferred from altimetry (Xu et al., 2015), are principally related to basin-scale changes in the subpolar North Atlantic. Across the northeast Atlantic over 1988-2007, we identify 25-50% reductions of meridional density gradients in the depth range 500-1000 m representative of a layer that supports geostrophic inflow to the Slope Current, which can be considered as "fed from the

25   west". In particular, we find abrupt reductions of density gradient over 1995-97, coincident with abrupt weakening of the Slope Current at the FASTNEt and EEL sections. Using a common framework, we find that changes in annual-mean wind forcing contribute around 20% to the density gradient variability. Changes in wind forcing, specifically the along-slope component of wind stress, are associated with the transition of the North Atlantic Oscillation (NAO) from a positive to a neutral phase during the mid-1990s, weakening wind forcing of the Slope Current at that time.

30   To summarize forcing mechanisms, the schematics in Fig. 14 indicate the density gradients, wind forcing, Ekman transports and sea surface slopes associated with weak and strong Slope Current transport. Strong (weak) transport is associated with a strong (weak) subpolar gyre, and the NAO in a positive (negative) phase. Emphasizing the conditions for strong Slope

Current transport: in the deep ocean, colder water to the north sets up a stronger northward density gradient, while the downward sea surface slope to the north steepens; stronger eastward geostrophic flow is supported by the combined effect of density gradient and strengthened along-slope (northward) winds and onshore Ekman transports; northward steepening of the cross-slope gradient in sea surface height becomes more pronounced in proportion to inflow recruited to the barotropic Slope

5   Current.

Downstream consequences of changes in Slope Current transport have also been investigated. Tracked forwards in the ORCA12 hindcast, a substantial number of particle trajectories reach the northern North Sea, and we accordingly diagnose the % of particle locations in the northwest and northeast North Sea, as metrics for Atlantic inflow in these regions. Over the 1988-2007 hindcast, we thus identify a decline from ~40% in the early 1990s to ~15% in the mid-2000s, accompanied by the

10   reductions in Slope Current transport and a freshening trend in the northern North Sea that is consistent with limited observations in the region (Hjøllo et al., 2009). Interannual variations in freshwater exchange with the Baltic Sea likely contribute to the observed salinity variations. There is a climatological seasonal variation of North Sea freshwater content by ~20%, with peak values in July/August that lag by 2-3 months the net fresh inflow from the Baltic, which in turn varies by a factor of ~3 over the seasonal cycle (see Sündermann and Pohlmann, 2011 - their Fig. 17).

15   While Baltic inflow dominates the seasonal cycle of salinity, Atlantic inflow dominates mean salinity of the North Sea (Sündermann and Pohlmann, 2011). A strong interannual influence of Atlantic inflow on North Sea salinity seems likely, given the high variability of this inflow, ~50% of which is mixed with fresher North Sea water (including Baltic outflow) before outflow in the Norwegian Coastal Current (Winther and Johannessen, 2006). The ORCA12 hindcast is unlikely to fully represent interannual variability of Baltic exchange, hence our focus here is on the Atlantic influence.

20   Variable Atlantic inflow to the North Sea has a likely impact on North Sea ecosystems via hydrographic changes, as previously suggested by Reid et al. (2001). The northern North Sea undergoes seasonal stratification, with associated patterns and timings of productivity (Sharples et al., 2006), which may be sensitive to the relative influence of Atlantic Water. Changes in of inflow prior to our study period may also explain a widely-documented ecosystem regime shift in the early 1980s that was observed in phytoplankton and zooplankton populations (Beaugrand, 2004).

25   Looking back over a longer period, to the late 1950s, we propose a proxy for Atlantic inflow in sea level records. Variability of Slope Current transport variability is evident in sea level differences between Lerwick (Shetland) and Torshavn (Faeroes), in both tide gauge records and a longer ORCA12 hindcast spanning 1958-2013. With locally strong isostasy, differences in local datums, and seasonal steric effects, there are considerable challenges in extracting from tide gauge records the signal that is associated with Slope Current transport. However, with reasonable agreement between SSH differences from the tide

30   gauge data and those from the model hindcast, the proxy suggests substantial multi-decadal variability in Slope Current transport and Atlantic inflow to the North Sea, as sampled over our shorter study period.

The larger scale context for long-term changes in the meridional density gradients that support the Slope Current, and Atlantic inflow to the North Sea, likely involves the basin-scale ocean circulation. Previous studies provide evidence for a decline of the Atlantic Meridional Overturning Circulation (AMOC) in mid-latitudes (at 48°N) between the early 1990s and

the mid 2000s (Balmaseda et al. 2007; Grist et al. 2009), while Josey et al. (2009) - see their Fig. 7b - show this decline to be representative across ~48-60°N, a zone encompassing Slope Current inflow (see Fig. 3). The striking shift to weaker Slope Current transport at the EEL section over 1996-98 (Fig. 4b) coincides with a major warming of the subpolar gyre at this time (Robson et al. 2012). More recently, there has been a major reversal of temperature in the eastern subpolar gyre along with

5 formation of a particularly dense mode of Subpolar Mode Water, associated with extreme cooling in the winter of 2013/14 (Grist et al., 2015), reinforced through further cooling during 2015 (Duchez et al., 2016). These transient events may have restored strong meridional density gradients, re-strengthened the Slope Current, and replenished the northern North Sea with Atlantic Water.

In conclusion, we hypothesize that recent weakening of the AMOC in mid-latitudes led to declines in meridional density
10 gradients (primarily due to warming in the eastern subpolar gyre), geostrophic inflow to the continental slope, and the Slope Current. The present study provides evidence that a variable fraction of Slope Current water crossing the Extended Ellett Line (EEL) is destined for the North Sea, on timescales of 3-6 months. Existing EEL observations additionally indicate warming and declining nutrient concentrations in the Rockall trough from 1996 to the mid-2000s (Johnson et al., 2013), which may have further influenced North Sea ecosystems that previously underwent a regime shift over 1982-88, from a
15 "cold dynamic equilibrium" (1962-83) to a "warm dynamic equilibrium" (1984-99) (Beaugrand, 2004). The new OSNAP monitoring array (http://www.o-snap.org/), spanning the subpolar gyre and incorporating EEL, should provide the observations needed to further investigate these changes in Slope Current transport and the downstream consequences.

Author Contribution

RM designed the study and undertook analysis of the ORCA12-N01 hindcast, including the Lagrangian diagnostics. SC
20 analysed the observations of mean absolute dynamic topography and climatological density. MI developed the wind forcing metric. MP analysed drifter observations and calculated the wind forcing metric. IH analysed tide gauge records at Lerwick and Torshavn. BM diagnosed the ORCA12-N06 hindcast. RM prepared the manuscript with contributions from all co-authors.

Acknowledgements

25 RM acknowledges the support of a 2013 Research Bursary awarded by the Scottish Association for Marine Science. MI and MP acknowledge the UK National Environment Research Council (NERC) programme FASTNEt (NERC Ref. NE/I030224/1). SC acknowledges the NERC project UK-OSNAP (NERC Ref. NE/K010700/1) and the EU-funded project NACLIM. BM acknowledges funding from NERC through the RAPID-AMOC Climate Change (RAPID) programme. The ORCA12 simulations were undertaken at the National Oceanography Centre, using the NEMO framework. NEMO is a state-
30 of-the-art, portable modelling framework developed by a consortium of European institutions, namely the National Centre

for Scientific Research (CNRS), Paris, the UK Met Office (UKMO), Mercator-Ocean and NERC. This study is in memory of Dr Kate Stansfield.

References

Amante, C., and B. W. Eakins, B. W.: ETOPO1 1 arc-minute global relief model: procedures, data sources and analysis. US

5 Department of Commerce, National Oceanic and Atmospheric Administration, National Environmental Satellite, Data, and Information Service, National Geophysical Data Center, Marine Geology and Geophysics Division Colorado, 2009.

AVISO+: SSALTO/DUACS User Handbook: (M)SLA and (M)ADT Near-Real Time and Delayed Time Products, SALP-MU-P-EA-21065-CLS, CLS-DPS-NT-06--34 (4rev2, 18/4/2014), 2014.

Balmaseda, M. A., Smith, G. C., Haines, K., Anderson, D., Palmer, T. N., and Vitard, A.: Historical reconstruction of the

10 Atlantic meridional overturning circulation from the ECMWF operational ocean reanalysis. Geophys. Res. Lett., 34, L23615, doi:10.1029/2007GL031645, 2007.

Beaugrand G.: The North Sea regime shift: evidence, causes, mechanisms and consequences. Progr. Oceanogr., 60, 245-262, 2004.

Blaker, A. T., Hirschi, J. J.-M., McCarthy, G., Sinha, B., Taws, S., Marsh, R., de Cuevas, B. A., Alderson, S. G., and A. C.

15 Coward, A.C.: Historical analogues of the recent extreme minima observed in the Atlantic meridional overturning circulation at 26°N. Clim. Dyn., 44, 457-473, doi:10.1007/s00382-014-2274-6, 2015.

Blanke B, and Raynaud, S.: Kinematics of the Pacific Equatorial Undercurrent: a Eulerian and Lagrangian approach from GCM results. J. Phys. Oceanogr., 27, 1038-1053, 1997.

Brodeau, L., Barnier, B., Treguier, A.-M., Penduff, T., and Gulev, S.: An ERA40-based atmospheric forcing for global ocean

20 circulation models. Ocean Model. 31, 88-104, 2010.

Burrows, M., and Thorpe, S. A.: Drifter observations of the Hebrides slope current and nearby circulation patterns. Ann. Geophysicae 17, 280-302, 1999.

Burrows, M., Thorpe, S. A., and Meldrum, D. T.: Dispersion over the Hebridean and Shetland shelves and slopes. Cont. Shelf Res., 19, 49-55, 1999.

25 Dee, D., Uppala, S., Simmons, A., Berrisford, P., Poli, P., Kobayashi, S., Andrae, U., Balmaseda, M., Balsamo, G., and Bauer, P.: The ERA-Interim reanalysis: Configuration and performance of the data assimilation system. Q. J. Roy. Met. Soc., 137 (656), 553-597, 2011.

Duchez, A., Frajka-Williams, E., Josey, S. A., Evans, D., Grist, J. P., Marsh, R., McCarthy, G. D., Sinha, B., Berry, D. I., and Hirschi, J. J.-M.: Drivers of exceptionally cold North Atlantic Ocean temperatures and their link to the 2015 European

30 heat wave. Environ. Res. Lett., 11(7), 074004, doi:10.1088/1748-9326/11/074004, 2016

Good, S. A., Martin M. J., and Rayner, N. A.: EN4: quality controlled ocean temperature and salinity profiles and monthly objective analyses with uncertainty estimates. J. Geophys. Res., 118, 6704-6716, doi:10.1002/2013JC009067, 2013.

Grist J. P., Marsh R., and Josey S. A.: On the relationship between the North Atlantic meridional overturning circulation and the surface-forced overturning stream function. J. Climate, 22, 4989-5002. doi:10.1175/2009JCLI2574.1, 2009.

Grist, J. P., Josey, S. A., Jacobs, Z. L., Marsh, R., Sinha, B., and van Sebille, E.: Extreme air-sea interaction over the North Atlantic subpolar gyre during the winter of 2013-14 and its sub-surface legacy. *Clim. Dyn.* (2015). doi:10.1007/s00382-015-2819-3, 2015.

Hecht, M. W., and Smith, R. D.: Toward a Physical Understanding of the North Atlantic: A Review of Model Studies in an Eddying Regime. Geophysical Monograph Series. American Geophysical Union 177, 213-239, 2013.

Hjøllo, S. S., Skogen, M. D., and Svendsen, E.: Exploring currents and heat within the North Sea using a numerical model, Journal of Marine Systems, 78 (1), 180-192, 2009.

Holgate, S.J., Matthews, A., Woodworth, P.L., Rickards, K.J., Tamisiea, M.E., Bradshaw, E., Foden, P.R., Gordon, K., Jevrejeva, S., Pugh, J.: New data systems and products at the Permanent Service for Mean Sea Level. J. Coastal Res., 29 (3), 493-504, 2013.

Huthnance, J. M.: Slope Currents and "JEBAR" J. Phys. Oceanogr., 14, 795-810, 1984.

Huthnance, J. M., Holt, J. T., and S. L.Wakelin: Deep ocean exchange with west-European shelf seas. Ocean Sci., 5, 621–634, www.ocean-sci.net/5/621/2009/, 2009.

Johnson, C., Inall, M., and S. Häkkinen: Declining nutrient concentrations in the northeast Atlantic as a result of a weakening Subpolar gyre. Deep Sea Research I, 82, 95-107, 2013.

Josey, S. A., Grist, J. P., and Marsh, R.: Estimates of meridional overturning circulation variability in the North Atlantic from surface density flux fields. J. Geophys. Res., 114, C09022, doi:10.1029/2008JC005230, 2009.

Large, W., and Pond, S.: Open ocean momentum flux measurements in moderate to strong winds. J. Phys. Oceanogr., 11 (3), 324-336, 1981.

MacKenzie, B. R., and Schiedek, D.: Daily ocean monitoring since the 1860s shows record warming of northern European seas, Global Change Biology, 13, 1335–1347, doi: 10.1111/j.1365-2486.2007.01360.x, 2007.

Madec, G.: NEMO ocean engine. Vol. 27 (Institut Pierre-Simon Laplace, France), 2008.

McClean, J. L., Poulain, P.-M., Pelton, J. W., and Maltrud, M. E.: Eulerian and Lagrangian statistics from surface drifters and a high-resolution POP simulation in the North Atlantic. J. Phys. Oceanogr. 32, 2472-2491, 2002.

Moat, B. I., and 11 others: Major variations in subtropical North Atlantic heat transport at short (5 day) timescales and their causes, J. Geophys. Res., 121, doi:10.1002/2016JC011660, 2016.

Petersen, M. R., Williams, S. J., Maltrud, M. E., Hecht, M. W., and Hamann, B.: A three-dimensional eddy census of a high-resolution global ocean simulation. J. Geophys. Res., 118, 1759-1774, 2013.

Permanent Service for Mean Sea Level (PSMSL): Tide Gauge Data, Retrieved 3 Nov 2015 from http://www.psmsl.org/data/obtaining/.

Reid, P. C., Holliday, N. P., and Smyth, T. J.: Pulses in eastern margin current with higher temperatures and North Sea ecosystem changes. Marine Ecology Progress Series, 215, 283-287, 2001.

Richter, K., O. H. Segtnan, and Furevik, T.: Variability of the Atlantic inflow to the Nordic Seas and its causes inferred from observations of sea surface height, J. Geophys. Res., 117, C04004, doi:10.1029/2011JC007719, 2012.

Rio, M. H., S. Guinehut, and Larnicol, G.: New CNES-CLS09 global mean dynamic topography computed from the combination of GRACE data, altimetry, and in situ measurements, J. Geophys. Res., 116, C07018, doi:10.1029/2010JC006505, 2011.

Robson, J., Sutton, R., Lohmann, K., Smith, D., and Palmer, M. D.: Causes of the rapid warming of the North Atlantic Ocean in the mid 1990s, J. Climate, 25, 2012.

Sharples, J., Ross O. N., Scott, B. E., Greenstreet, S., Fraser, H.: Interannual variability in the timing of stratification and the spring bloom in the north-western North Sea. Cont. Shelf Res., 26, 733–751, 2006.

Sherwin, T. J., Hughes, S. L., Turrell, W. R., Hansen, B., and Østerhus, S.: Wind-driven monthly variations in transport and the flow field in the Faroe–Shetland Channel, Polar Research, 27, 7–22, 2008.

Simpson, J. H., and Sharples, J.: Introduction to the Physical and Biological Oceanography of Shelf Seas, Cambridge University Press, 2012.

Sündermann, J., and Pohlmann, T.: A brief analysis of North Sea physics, Oceanologia, 53 (3), 663-689, doi:10.5697/oc.53-3.663, 2011.

Winther, N. G., and Johannessen, J. A.: North Sea circulation: Atlantic inflow and its destination, J. Geophys. Res., 111, C12018, doi:10.1029/2005JC003310, 2006.

Xu, W., Miller, P. I., Quartly, G. D., and Pingree, R. D.: Seasonality and interannual variability of the European Slope Current from 20 years of altimeter data with in situ measurement comparisons, Remote Sens. Env., 162, 196-207. doi:10.1016/j.rse.2015.02.008, 2015.

Table 1. Long-term mean and standard deviation (SD) of transport at the three selected sections along the continental shelf break, and corresponding age statistics for the two "downstream" sections. For details of the FASTNEt section, see Sect. 2.3. The EEL section is centred on 9.75°W, 57.25°N. The Shetland Shelf section is centred on 2.75°W, 60.75°N.

Section	Transport (Sv)		Travel Time (days since 1 January)		Travel Time (days since 1 July)	
	mean	SD	mean	SD	mean	SD
FASTNEt section	2.79	1.68	0.00	n/a	0.00	n/a
EEL section	2.95	2.03	19.4	7.7	28.7	20.4
Shetland Shelf	4.72	1.44	90.4	23.7	98.6	32.3
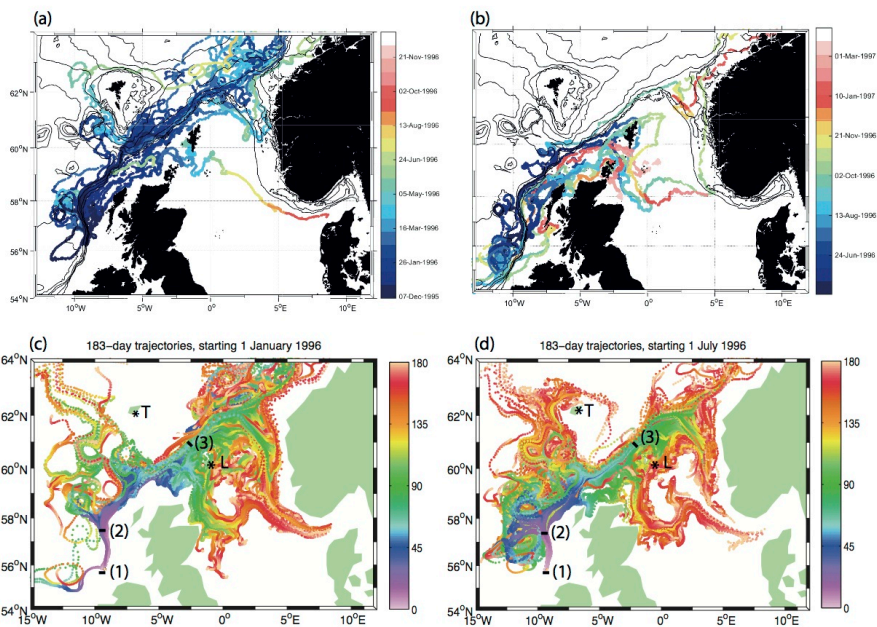
Figure 1: Drogued drifters released in (a) December 1995, (b) May 1996; model particle trajectories spanning 6 months, released on (c) 1 January 1996, (d) 1 July 1996 (630 model trajectories are plotted in each case). Drifters are colour-coded by calendar date. Model particles are colour-coded by age (days). Note that the drifter data span slightly different durations: up to 11 months, December 1995 – November 1996 (Fig. 1a); up to 10 months, May 1996 – March 1997 (Fig. 1b). In (c) and (d), we also indicate the sections west and north of Scotland – (1) FASTNEt; (2) EEL; (3) Shetland Shelf – used to diagnose Slope Current pathways and transports, and the locations of Lerwick (L) and Torshavn (T) where we take sea surface height to develop a proxy of Slope Current transport.
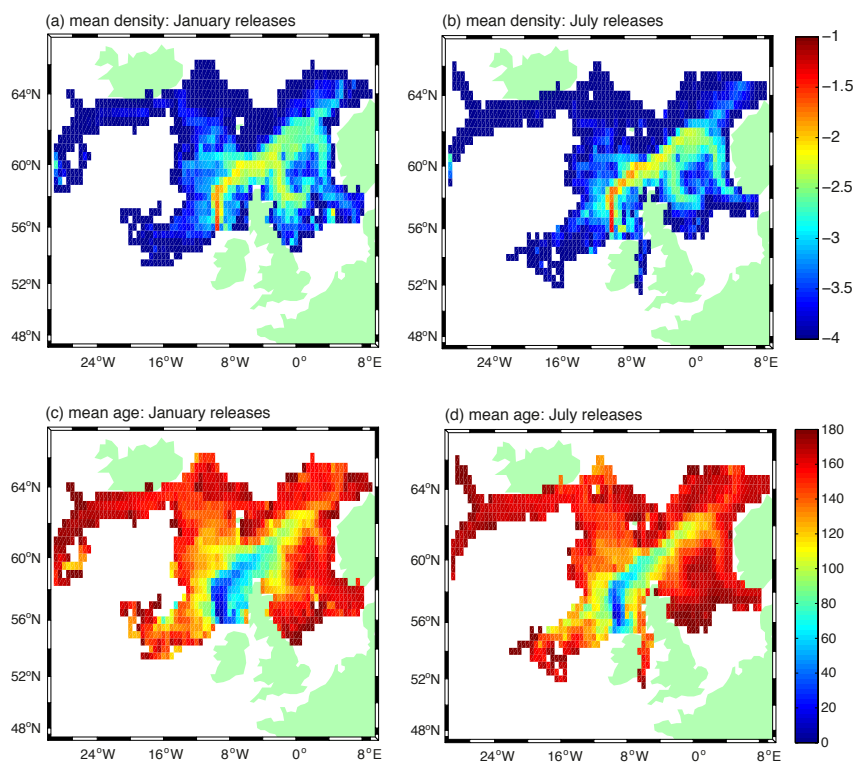
Figure 2: Forward trajectories from the FASTNEt section in ORCA12-N01: (a), (b) mean particle density for particles released on 1 January and 1 July; (c), (d) mean particle age for particles released on 1 January and 1 July. Averages are for 1988-2007, and values are binned at 0.5° x 0.5° resolution. Particle density is expressed as a fraction, obtained as the number of particle occurrences per 0.5° x 0.5° grid cell divided by the total number of particle occurrences. Ages are expressed as days since 1 January or 1 July. Note the log scale used for particle density.
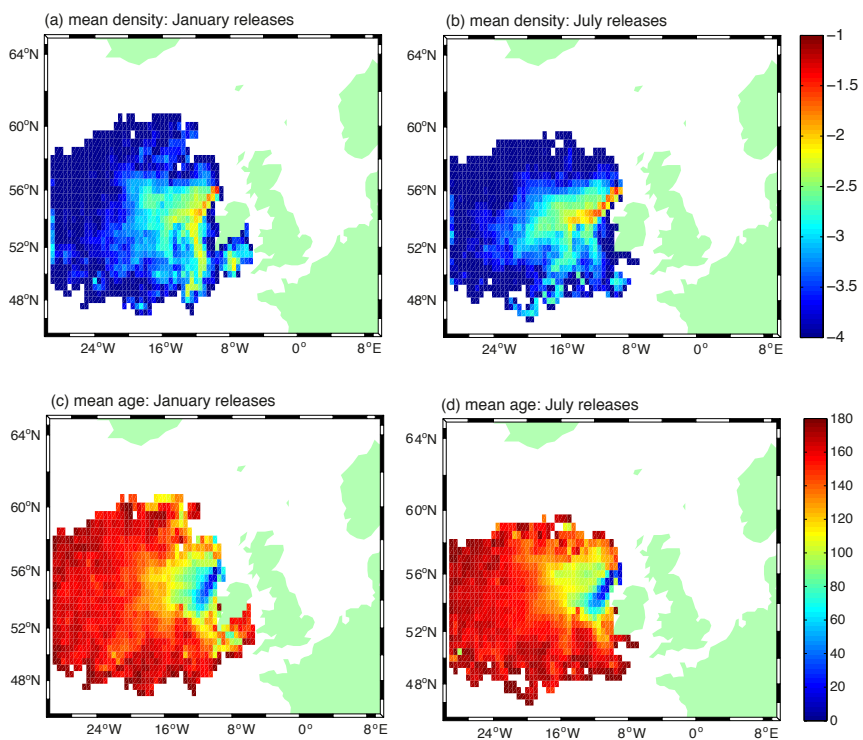
Figure 3: As Fig. 2, for backward trajectories.
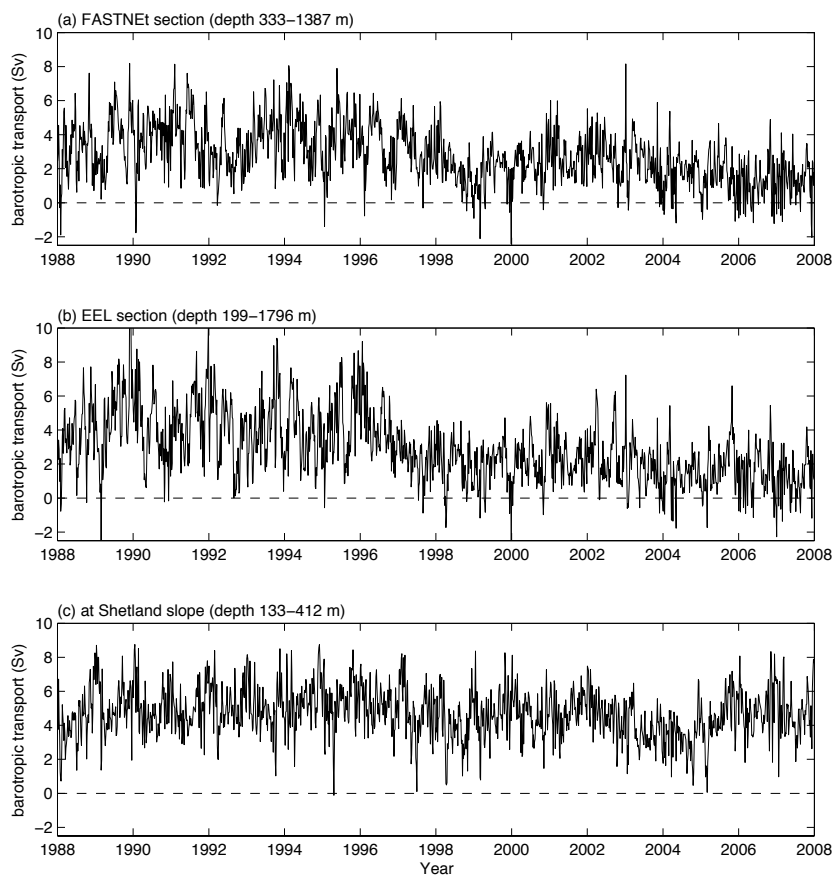
Figure 4: Slope Current transport at FASTNEt, EEL and Shetland Slope sections, 5-day averaged over 1988-2007 in ORCA12-N01.
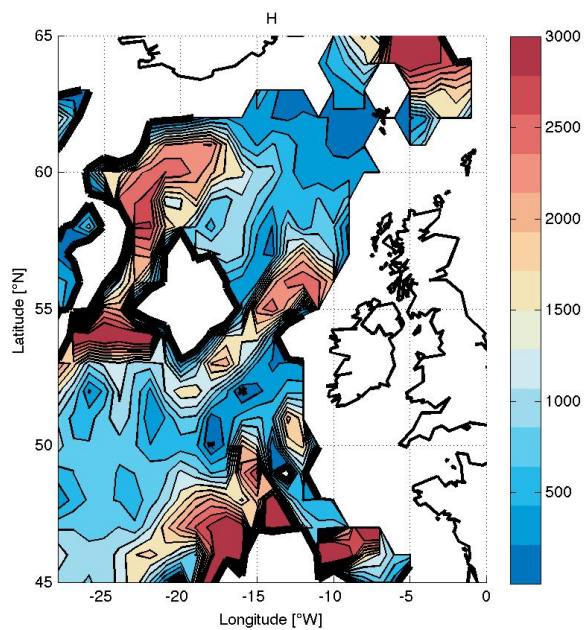
Figure 5: The depth scale *H* of Eq. (7), predicted from the meridional gradients of density and sea surface height; *H* is set to the local water depth, where *H* exceeds that depth; white areas inside the bold black contour indicate where *H* is negative (undefined).
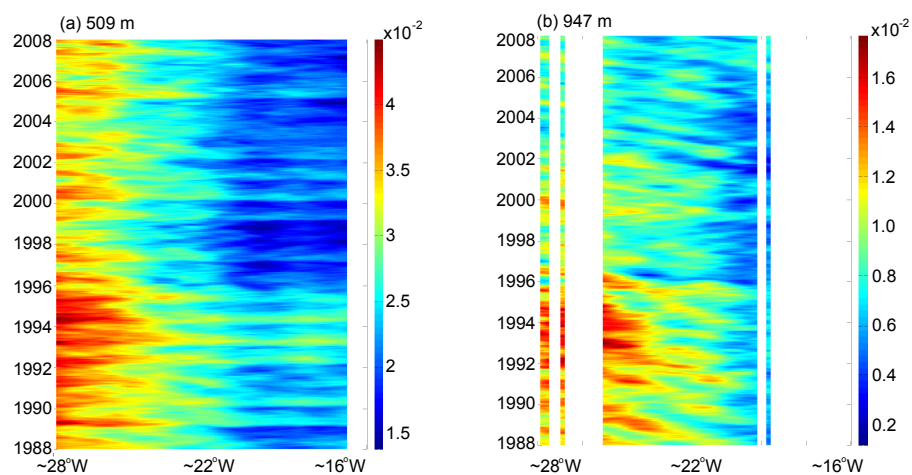
Figure 6: The northward trend of density (10^{-2} kg m^{-3} degree^{-1}, regressed in the latitude range 45-62°N) in the northeast Atlantic (in the approximate longitude range 16-28°W), 5-daily for 1988-2007: (a) at 509 m; (b) at 947 m.
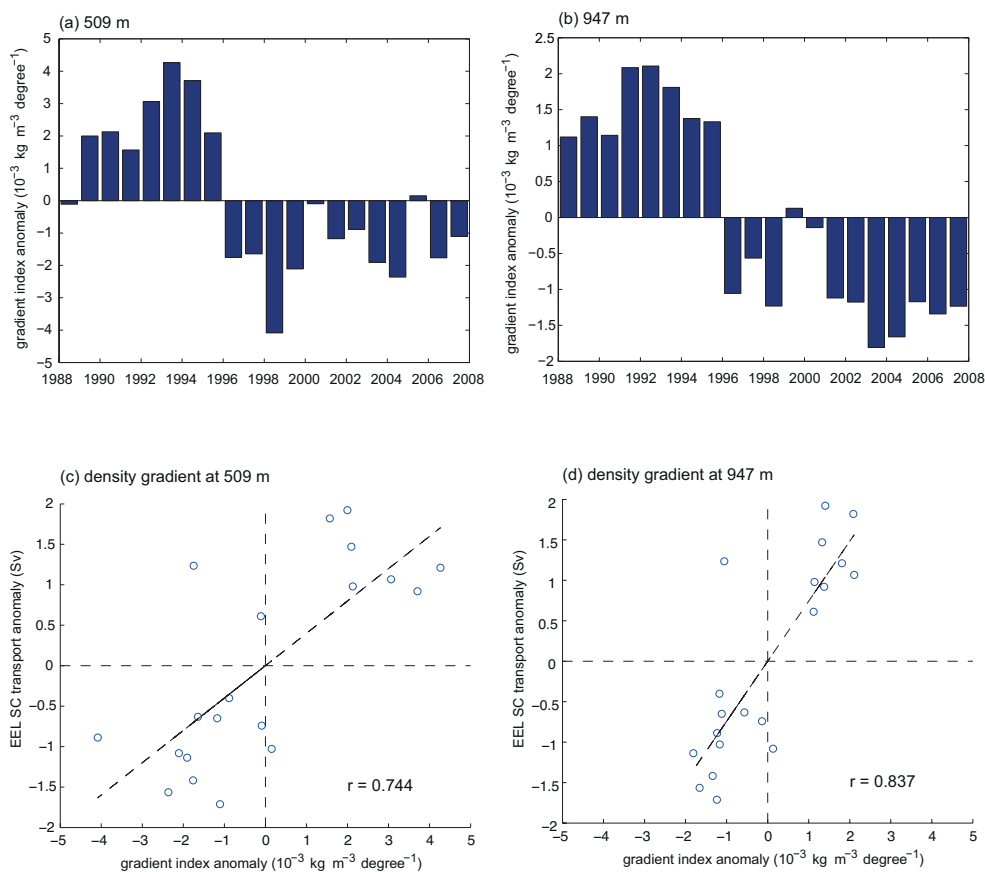
Figure 7: Time series over 1988-2007, in ORCA12-N01, of anomalies in density gradients averaged across 15-28°W and annually, for 509 m (a) and 947 m (b), and (c), (d), plotted against annual-mean Slope Current (SC) transports at the EEL section.
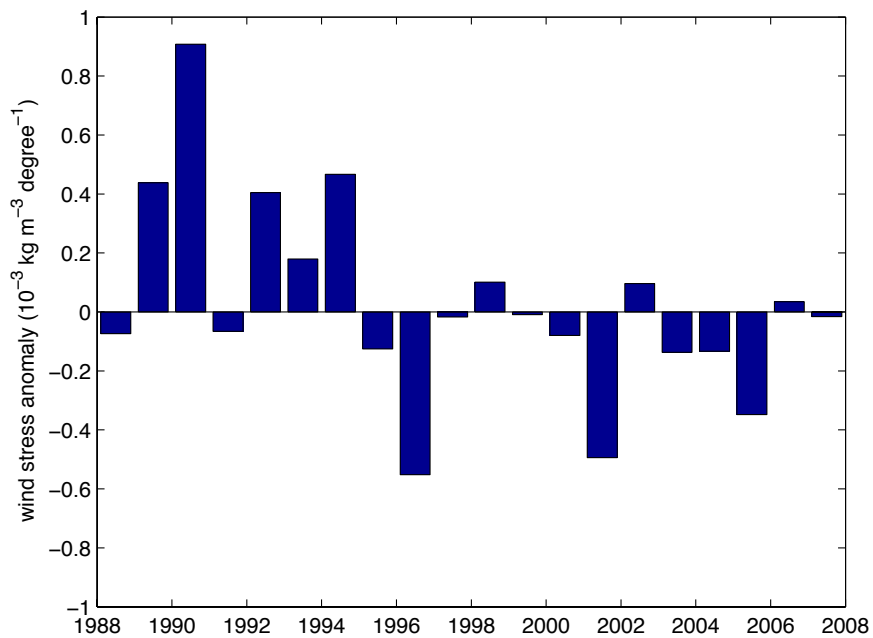
Figure 8: The wind forcing metric, expressed in units of northward density gradient (10^{-2} kg m^{-3} degree^{-1}, regressed in the latitude range 48-62°N) - see text for details.
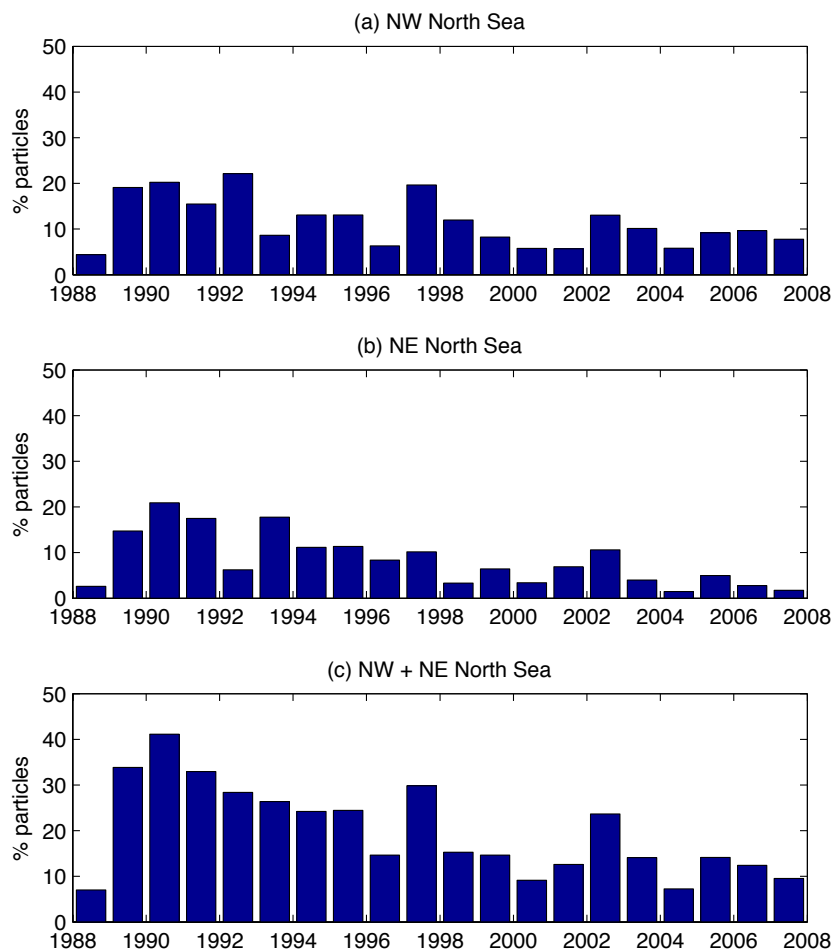
Figure 9: Histograms (per year) of mean fraction of (combined) January and July released particles residing: (a) in the northwest North Sea (4.5°W to 1.5°E, south of 59°N); (b) in the northeast North Sea (east of 1.5°E, south of 62°N); (c) the combined total.
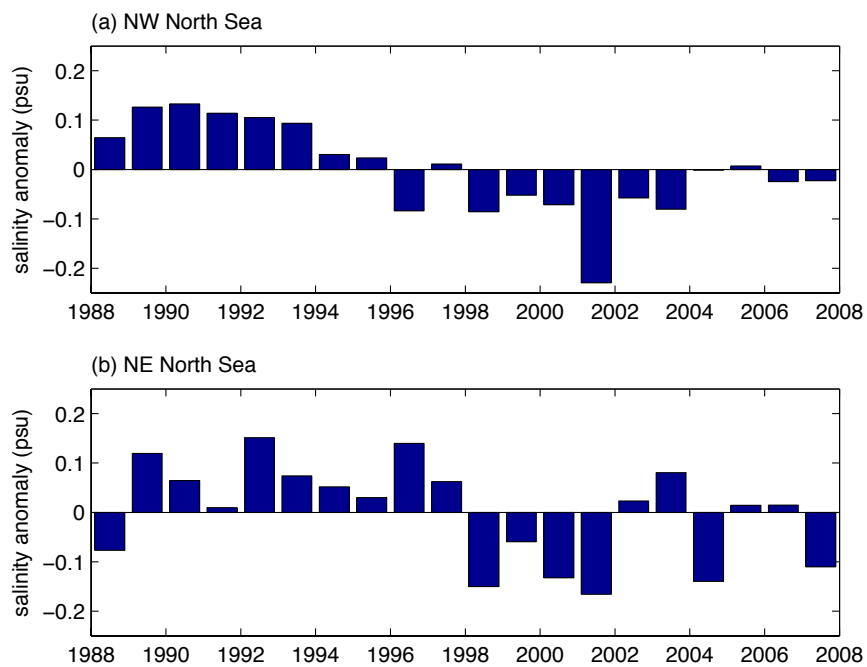
Figure 10: Area and annually averaged surface salinity anomalies, in northwest and northeast sectors of the North Sea over 1988-2007 in ORCA12-N01.
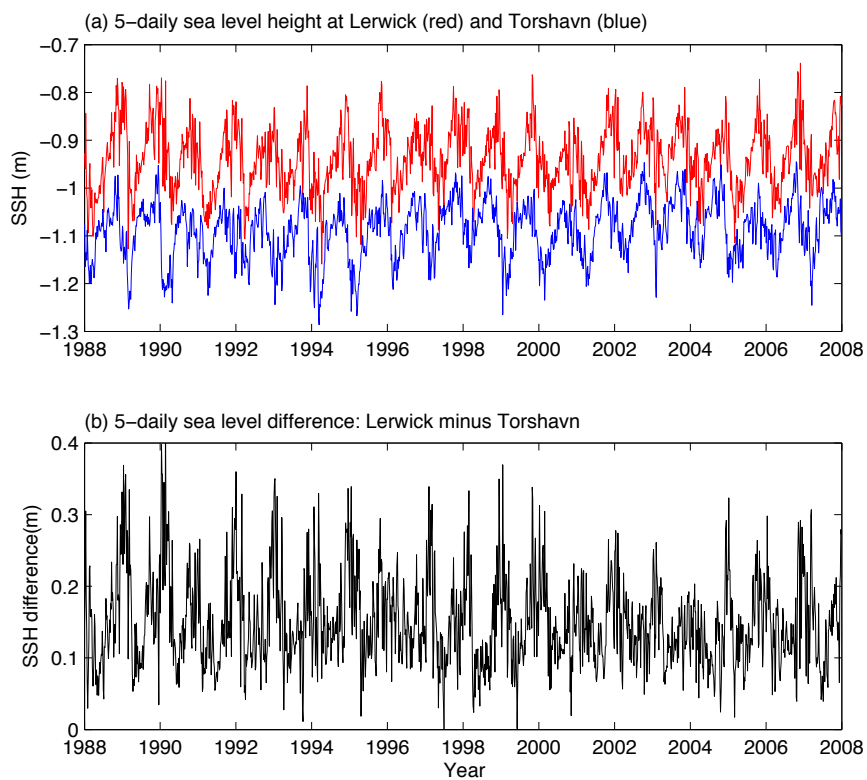
Figure 11: Relative sea surface height at Lerwick and Torshavn, and the difference, 5-daily averaged over 1988-2007 in ORCA12-N01.
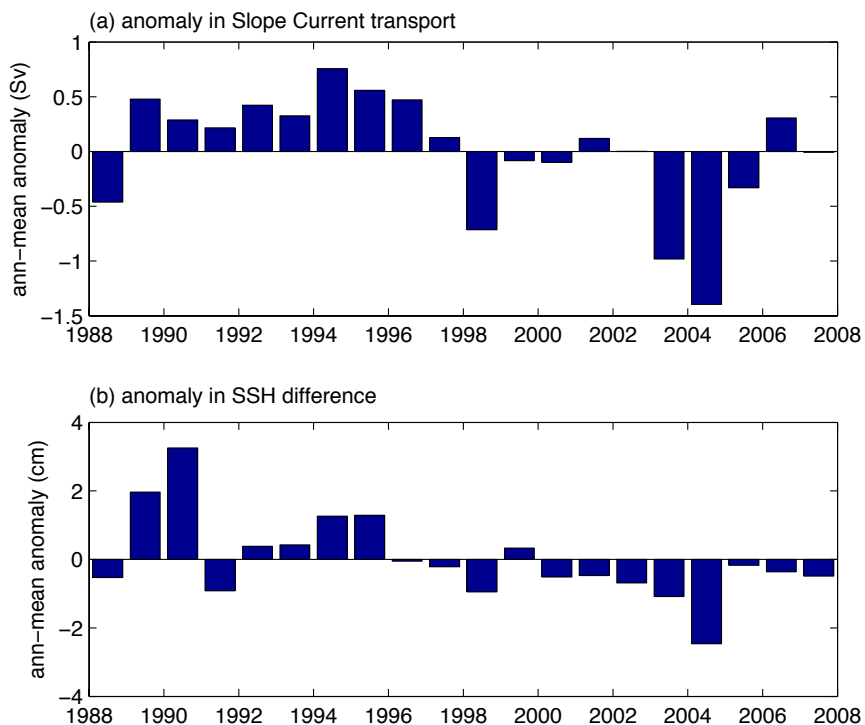
Figure 12: Annual-mean anomalies over 1988-2007, in ORCA12-N01, of: (a) Slope Current transport at the Shetland Shelf; (b) Lerwick-Torshavn SSH difference.
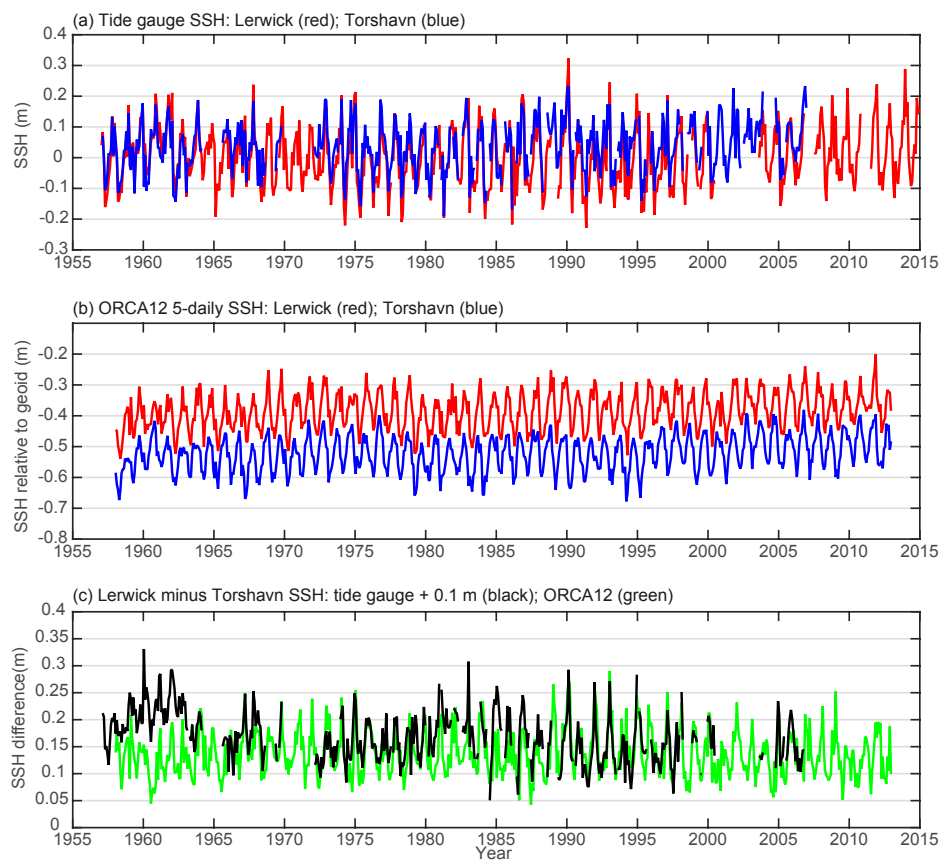
Figure 13: Monthly-mean sea surface height at Lerwick and Torshavn: (a) in tide gauge records (1957 onwards); (b) in ORCA12-N06 (1958-2013); (c) differences, Lerwick minus Torshavn.

(a) Weak Slope Current
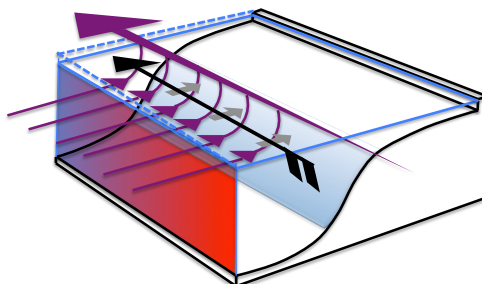
(b) Strong Slope Current
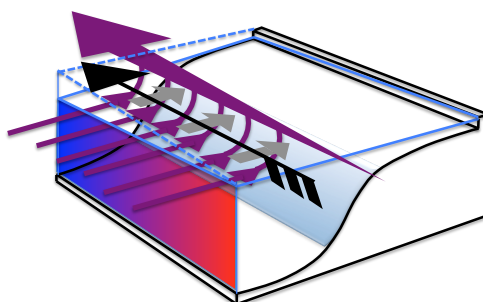
Figure 14: Schematics showing density gradients (shaded red to pale/dark blue), eastward geostrophic inflow, wind forcing (black alongshore arrow), Ekman transports (grey onshore arrows) and sea surface slopes at an idealized eastern boundary, associated with (a) weak and (b) strong Slope Current transport.